# Hydrophobicity versus pore size: polymer coatings to improve membrane wetting resistance for membrane distillation

Allyson L. McGaugheya, Prathamesh Karandikarb, Malancha Guptab, and Amy E. Childressa, \*

- <sup>a</sup> Sonny Astani Department of Civil and Environmental Engineering, University of Southern California, 3620 S. Vermont Avenue, Los Angeles, California 90089, United States
- <sup>b</sup> Mork Family Department of Chemical Engineering and Materials Science, University of Southern California, 925 Bloom Walk, Los Angeles, California 90089, United States

\*E-mail: amyec@usc.edu

## **Abstract**

Initiated chemical vapor deposition (iCVD) was used to coat two porous substrates (i.e., hydrophilic cellulose acetate (CA) and hydrophobic polytetrafluoroethylene (PTFE)) with a crosslinked fluoropolymer to improve membrane wetting resistance. The coated CA membrane was superhydrophobic and symmetric. The coated PTFE membrane was hydrophobic and asymmetric, with smaller pore size and lower porosity on the top surface than on the bottom surface. Membrane performance was tested in membrane distillation experiments with (1) a high-salinity feed solution and (2) a surfactant-containing feed solution. In both cases, the coated membranes had higher wetting resistance than the uncoated membranes. Notably, wetting resistances were better predicted by LEP distributions than by minimum LEP values. When LEP distributions were skewed towards high LEP values (i.e., when small pores with high LEP were greater in number), significant (measurable) salt passage did not occur. For the high-salinity feed solution, the coated PTFE membrane had greater wetting resistance than the coated CA membrane; thus, reduced surface pore size/porosity (which may reduce intrapore scaling) was more effective than increased surface hydrophobicity (which may reduce surface nucleation) in preventing scaling-induced wetting. Reduced pore size/porosity was equally as effective as increased hydrophobicity in resisting surfactant-induced wetting. However, reduced porosity can negatively impact water flux; this represents a permeability/wetting resistance tradeoff in membrane distillation – especially for high-salinity applications. Membrane and/or membrane coating properties must be optimized to overcome this permeability/wetting resistance tradeoff and make MD viable for the treatment of challenging streams. Then, increasing hydrophobicity may not be necessary to impart high wetting resistance to porous membranes. These results are important for future membrane design, especially as manufacturers seek to replace perfluorinated materials with environmentally friendly alternatives.

**Keywords:** initiated chemical vapor deposition, porous membranes, coating, hydrophobicity, membrane distillation

## 1. Introduction and Background

Membrane distillation (MD) is a promising option for applications requiring treatment of high-salinity wastewaters, high water recovery, or brine concentration.<sup>1,2</sup> Unlike reverse osmosis, MD is only slightly affected by feed water salinity because MD relies on a vapor pressure driving force;<sup>3,4</sup> also, MD can achieve high rejection of low-molecular-weight solutes that may pass through reverse osmosis membranes.<sup>5-7</sup> Unlike conventional thermal distillation, MD can easily integrate with low-grade waste heat and solar thermal power;<sup>1,8-11</sup> MD can also be more energy-efficient at small system capacities.<sup>1</sup>

Generally, microporous, hydrophobic, polymer membranes are used in MD; these are often composed of polytetrafluoroethylene (PTFE), polyvinylidene fluoride, or polypropylene.<sup>12</sup> The vapor pressure difference across the membrane drives water from a warmer, saline feed stream to evaporate at the membrane surface and diffuse through the membrane pores.<sup>1</sup> In MD, permeability and water flux are known to increase with increasing membrane porosity and to decrease with increasing membrane thickness.<sup>1</sup> Increasing membrane pore size also increases permeability,<sup>1</sup> although researchers have observed that water flux is less sensitive to pore size than to porosity and thickness, especially at pore sizes less than 0.3 μm.<sup>3</sup>

When the membrane pores are unwetted, a vapor gap separates the feed and distillate streams and prevents the passage of non-volatile solutes.<sup>1,6</sup> However, pore wetting does occur and is frequently associated with salt precipitation (scaling) on the membrane surface<sup>13</sup> and/or the presence of surfactants in the feed stream.<sup>14,15</sup> Pore wetting and subsequent solute passage can be predicted by the wetting resistance of a membrane. Increased wetting resistance is a key goal of many studies on new MD membrane materials and/or coatings (e.g., Su et al.<sup>16</sup>, Karanikola et al.<sup>17</sup>, Wang and Lin<sup>18</sup>, Boo et al.<sup>19</sup>, Servi and colleagues<sup>20,21</sup>, Warsinger et al.<sup>22</sup>).

## 1.1. Current understanding of membrane wetting

Wetting can occur partially through a membrane or fully, through its depth. In partial wetting, the feed solution enters the pore and reduces the vapor gap thickness. This can lead to full wetting via liquid bridging across the thin vapor gap.<sup>23</sup> When the pore is fully wetted (i.e., there is no vapor gap), the feed and distillate solutions can mix and solutes can pass through the membrane.<sup>15</sup>

Expectations of wetting resistance are often based on membrane hydrophobicity, which is typically characterized by surface contact angle ( $\theta$ ) measurement. Generally, a membrane is expected not to wet if it is hydrophobic (i.e., has low surface energy with  $\theta > 90^{\circ}$ ) and is expected to wet if it is hydrophilic (i.e., has high surface energy with  $\theta < 90^{\circ}$ ). The maximum achievable contact angle for static water on a smooth surface (i.e., the maximum contact angle due to material surface energy alone) is  $120^{\circ}.^{24,25}$  However, contact angle measurements also depend on surface roughness;<sup>26</sup> on hydrophobic surfaces, increased roughness increases the measured contact angle.<sup>25,27</sup> Low-energy surfaces that are rough can be "superhydrophobic", (i.e., have  $\theta \ge 150^{\circ}$ ). As polymeric membrane surfaces are generally rough, superhydrophobic MD membranes are most often produced using low-surface-energy materials or coatings

that reduce surface energy (e.g., Su et al.<sup>16</sup>, Karanikola et al.<sup>17</sup>, Servi and colleagues<sup>20,21</sup>, Warsinger et al.<sup>22</sup> Sadeghi et al.<sup>26</sup>, Munirasu et al.<sup>28</sup>, Wang et al.<sup>29</sup>, Li et al.<sup>30</sup>, Liao et al.<sup>31</sup>, Guo et al.<sup>32</sup>, Dong and colleagues<sup>33,34</sup>, Hamzah and Leo<sup>35</sup>, Zhu et al.<sup>36</sup>, Cong and Guo<sup>37</sup>, Meng and colleagues<sup>38,39</sup>, Lu et al.<sup>40</sup>, Xiao and colleagues<sup>41,42</sup>); some of these coatings also increase surface roughness. A few researchers (e.g., Munirasu et al.<sup>28</sup>, Wang et al.<sup>29</sup>, Li et al.<sup>30</sup>) have also produced superhydrophobic MD membranes specifically via patterned surface microstructures on polymer membranes.

Membrane wetting resistance is also often quantified by liquid entry pressure (LEP), and it is assumed that if the transmembrane pressure exceeds the LEP, the feed solution will flood the membrane pore(s). In the MD literature, LEP is most frequently modeled by the Young-Laplace equation for a single pore:

$$LEP = \frac{-2B\gamma_{lv}\cos(\theta)}{r} \tag{1}$$

where B is a pore geometry factor (equal to one for cylindrical pores),  $\gamma_{lv}$  is liquid-vapor surface tension of the wetting phase, and r is pore radius.  $\theta$  has been defined as the surface contact angle,<sup>43</sup> the surface advancing contact angle,<sup>44</sup> the intrinsic contact angle (i.e., between the feed solution and a smooth sample of membrane material),<sup>45</sup> and the intrinsic advancing contact angle.<sup>21</sup>

For PTFE membranes, which typically consist of strands of polymer material (fibrils) connected at nodes,  $^{12}$  Kim and Harriott  $^{46}$  developed a model to describe wetting through a grid of fibrils of radius R that form pores of radius r:

$$LEP = \frac{-2\gamma_{lv}}{r} \frac{\cos(\theta - \alpha)}{1 + \frac{R}{r}(1 - \cos\alpha)}$$
 (2)

where  $\alpha$  is the angle formed by the meniscus of the wetting liquid penetrating the pore. According to the Kim and Harriott model,<sup>46</sup> wetting resistance depends on the surface pore size. It is assumed that large surface pores connect to various internal pores without bottlenecks. For membranes characterized by interconnected internal pore structures and relatively high (e.g., 50%) porosities, such as the PTFE and CA membranes used in the current study, internal bottlenecks are unlikely.<sup>46</sup> Guillen-Burrieza et al.<sup>45</sup> found good agreement between experimental and theoretical results for the Kim-Harriott model using a range of membranes, with R/r determined from atomic force microscopy (AFM) results and  $\theta$  as the intrinsic advancing contact angle.

In previous studies, membrane LEP has typically been defined as a single value - the minimum LEP - which represents wetting of the largest membrane pore. However, typical membranes are comprised of a range of pore sizes and are characterized by a pore size distribution. During MD operation, wetting can only be detected if sufficient solute passage occurs. It is likely that in real systems, wetting of multiple pores - rather than the single largest pore - occurs before wetting is detected and becomes disruptive. Similarly, the experimental LEP depends on the sensitivity of the measured response parameter. Previous researchers have used various response parameters to detect wetting and LEP exceedance, such as continuous flow,<sup>3</sup> an increase in distillate conductivity,<sup>21</sup> and visual observation of a droplet<sup>45</sup> or droplets.<sup>46</sup> If distillate flowrate

is used, for example, enough pores must be wetted for the flow to be detectable. Again, wetting of multiple pores – rather than the single largest pore – may occur before wetting is detected.

In real systems, the theoretical minimum LEP (representing wetting of the single largest pore) may not be of practical importance. Expressing LEP as a distribution, analogous to the pore size distribution, may provide greater understanding and ability to consistently characterize wetting resistance. LEP distributions have not previously been reported in the literature, to the best of our knowledge.

## 1.1.1. Scaling-induced wetting

Scaling hydrophilizes the membrane surface and reduces the LEP. Scaling occurs due to salt crystal nucleation and growth. Nucleation will theoretically occur in any supersaturated system given sufficient time.<sup>47</sup> Nucleation occurs when the Gibbs free energy barrier to nucleation ( $\Delta G^*$ ) is exceeded. Nucleation is either primary or secondary (i.e., nucleation on existing crystals). Primary nucleation occurs either homogeneously, in pure solution, or heterogeneously on a foreign surface (e.g., a membrane surface).<sup>47</sup> The resistance of the membrane to scaling is generally quantified by the Gibbs free energy barrier to heterogeneous nucleation on the membrane surface ( $\Delta G_M^*$ ).<sup>17,47,48</sup>

Although surface scaling is often associated with wetting in MD,<sup>15</sup> some researchers suggest that surface scaling alone does not lead to wetting but that internal scaling is required for pore wetting to occur.<sup>23,49</sup> Intrapore scaling causes the pores to have hydrophilic surfaces that may facilitate liquid penetration.<sup>23,49</sup> Intrapore scaling can begin with surface scaling, via secondary nucleation on existing crystals, or it can occur directly via intrapore nucleation, which is when crystals nucleate in pores or on pore walls. Nucleation occurs in the aqueous phase;<sup>47</sup> therefore, intrapore nucleation can only occur when the pores are partially wetted.

In previous studies, researchers have mainly focused on increasing the surface hydrophobicity of MD membranes to reduce scaling and scaling-induced wetting<sup>13</sup> (e.g., Su et al. <sup>16</sup>, Karanikola et al. <sup>17</sup>, Meng and colleagues <sup>38,39</sup>, Xiao and colleagues <sup>41,42</sup>). It has been suggested that increasing the surface hydrophobicity can prevent or delay scaling-induced wetting by increasing  $\Delta G_M^*$ . <sup>13</sup> This has also been observed experimentally; in 2018, Karanikola et al. <sup>17</sup> developed a superhydrophobic "slippery" membrane with high  $\Delta G_M^*$  and in 2019, Xiao et al. <sup>41</sup> developed a superhydrophobic, micropillared slippery membrane. Under scaling conditions, the superhydrophobic, "slippery" membranes outperformed commercial membranes, but eventually wetted. Interestingly, by comparing between superhydrophobic and superhydrophobic, "slippery" membranes, Xiao et al. <sup>42</sup> observed that that  $\Delta G_M^*$  may be less important than feed solution hydrodynamics, which were affected by the surface patterns on the slippery membrane, for controlling scaling (and, therefore, scaling-induced wetting).

Also, in MD, it has been reported that membrane scaling is dominated by crystal deposition (e.g., deposition of crystals formed by secondary nucleation on surfaces in solution, such as colloidal particles) rather than heterogeneous nucleation on the membrane itself.<sup>22</sup> In this case, scaling could occur regardless of  $\Delta G_M^*$ .

and the efficacy of superhydrophobic membranes would be limited. This is important for real systems with more complex feed streams. In these cases, an alternative membrane modification strategy may be necessary. Gryta<sup>23</sup> found that scaling-induced wetting could be mitigated by a low-porosity surface layer, which sterically restricted intrapore crystal growth. However, the low-surface-porosity membrane was not compared to a superhydrophobic membrane. To the best of our knowledge, our current study represents the first comparison of the efficacy of superhydrophobic and small-pore-size/low-porosity membranes to prevent scaling-induced wetting in MD. We hypothesize that reduced surface pore size and/or porosity (which may reduce intrapore scaling) can be as - or more - effective than increased surface hydrophobicity (which may reduce surface nucleation) in preventing scaling-induced wetting.

## 1.1.2. Surfactant-induced wetting

When considering applications requiring treatment of challenging streams (e.g., desalination of produced waters from oil and gas operations), the presence of surfactants in the feed solution is also a concern.<sup>19</sup> Surfactant molecules can adsorb to a hydrophobic membrane surface with the hydrophilic head outward, which effectively hydrophilizes the surface.<sup>50,51</sup> Surfactants can also reduce the surface tension of the feed solution, which reduces the LEP. If the LEP is sufficiently low at a pore entrance, partial wetting will occur. After partial wetting occurs, surfactant molecules can readily adsorb to and hydrophilize the wetted portion of the pore walls. As additional surfactant molecules are transported to the liquid-vapor interface, the local surfactant concentration increases and the surface tension of the feed solution decreases further. This can eventually lead to full wetting of the membrane.<sup>51</sup>

Similar to scaling-induced wetting prevention, most previous researchers have focused on modifying membrane surface hydrophobicity to prevent surfactant-induced wetting. Superhydrophobic membranes and omniphobic membranes (i.e., hydrophobic membranes with re-entrant or concave pore openings that provide further wetting resistance) have generally shown improved resistance to surfactant-induced wetting during short-term operation (e.g., <sup>18,19,52</sup>). Superoleophobic (i.e., highly oil-repellant) membranes and hydrophilic/oleophobic coatings on omniphobic substrates have also prevented surfactant-induced wetting for up to 10 h (e.g., <sup>53,54</sup>). Amphiphobic membranes (i.e., membranes that are both hydrophobic and oleophobic) have shown improved resistance to wetting by oil- and surfactant-containing feed solutions. <sup>55</sup> However, the ability of small-pore-size and/or low-porosity membranes to mitigate surfactant-induced wetting has not been studied, to the best of our knowledge. We hypothesize that reducing surface pore size and/or porosity may be as effective as increasing surface hydrophobicity to prevent surfactant-induced wetting.

#### 1.2. Membrane modification

Notably, previous studies have focused on improving wetting resistance by increasing surface hydrophobicity, likely in an effort to maintain high water flux. Improving wetting resistance by reducing the membrane pore size may reduce water flux – especially if reducing the pore size also reduces the porosity.

This represents a permeability/wetting resistance tradeoff in MD. The permeability/wetting resistance tradeoff in MD is similar to the permeability/selectivity tradeoff in other membrane processes (e.g., reverse osmosis). However, in MD, solute selectivity is lost when pore wetting occurs: this represents a step change in selectivity that is unlike the continuous decrease in selectivity with increasing permeability that exists for processes like reverse osmosis. Another example of the permeability/wetting resistance tradeoff in MD is operation at low flux when treating high-salinity feed solutions, which is done to reduce concentration polarization and scaling that reduce membrane wetting resistance. <sup>2,15</sup>

Superhydrophobic membranes are most commonly fabricated by coating substrates with low-surface-energy materials (e.g., Su et al. 16, Karanikola et al. 17, Servi and colleagues 20,21, Warsinger et al. 22, Sadeghi et al. 26, Liao et al. 31, Guo et al. 32, Dong and colleagues 33,34, Hamzah and Leo 35, Zhu et al. 36, Cong and Guo 37, Meng and colleagues 38,39, Lu et al. 40). However, many coatings previously considered to be "gold standards" for imparting superhydrophobicity consist of long-chain, perfluorinated compounds (e.g., 17,21,22,26,32-37) that have been listed as precursors to perfluorooctanoic acid (PFOA). 57 PFOA is an environmentally persistent, toxic compound of increasing regulatory concern. 21 Although some superhydrophobic membranes have been fabricated using fluorinated compounds not listed as PFOA precursors, 16,20,31,38-40 these membranes have not been challenged by scaling- and surfactant-induced wetting conditions. To replace perfluorinated materials with suitable alternatives for membrane processes, it is important to mechanistically understand how the imparted properties delay or prevent wetting as well as identify properties that may be more desirable.

Initiated chemical vapor deposition (iCVD) is a vapor-phase process that can be used to produce a wide range of polymer coatings on textured substrates. iCVD does not require organic solvents, which makes it more environmentally friendly and simpler to operate<sup>24,58</sup> than other methods to produce superhydrophobic surfaces, which are mostly solvent-based.<sup>59</sup> Recently, iCVD was shown to be viable for roll-to-roll processing, making it an attractive option for large-scale functionalization of membranes. 60 In iCVD, vaporphase monomer and initiator radicals diffuse to and adsorb on a cooled substrate from the top down; polymerization occurs on the surfaces and pore walls of the cooled substrate. 20,24,58 For porous substrates, conformality (i.e., the evenness of coating thickness from the top to bottom of the substrate) is a key parameter. Nonconformal films, for which coating thickness decreases with depth, are formed when initiator radicals and/or monomer molecules are depleted at pore entrances.<sup>20,58</sup> In iCVD, coating conformality generally increases with decreasing fractional monomer saturation in the reactor, 20,58 and non-conformality generally increases with increasing aspect (length-to-diameter) ratio of the substrate pores.<sup>20</sup> Coating conformality can affect permeability. For coated membranes with the same surface pore size, permeability increases as conformality decreases. However, increasing pore density has a greater effect on increasing permeability than reducing conformality.<sup>20</sup> The effect of conformality on membrane wetting resistance for scaling- and surfactant-induced wetting conditions has not been investigated, to the best of our knowledge.

#### 1.3. Objectives

In this study, we use iCVD to coat a hydrophilic CA and hydrophobic PTFE substrate with poly(1H,1H,2H,2H-perfluorodecyl acrylate-co-ethylene glycol diacrylate) (P(PFDA-co-EGDA)), a crosslinked low-surface-energy material. Poly(1H,1H,2H,2H-perfluorodecyl acrylate) (PPFDA) coatings have been previously shown to be highly effective in MD applications<sup>21,22,32</sup> but these coatings, like P(PFDA-co-EGDA), are now considered unsuitable for commercial use due to PFOA concerns.<sup>21</sup> We compare coating conformality on the hydrophilic and hydrophobic substrates and test the uncoated and coated membranes to assess their ability to prevent scaling- and surfactant-induced wetting in MD. For the first time, the effectiveness of reduced pore size/porosity is compared with increased hydrophobicity to prevent scaling- and surfactant-induced wetting. The LEP distribution concept is proposed and evaluated to characterize membrane wetting resistance. Surface and performance characterization are performed to identify key membrane modification strategies to increase wetting resistance, challenging past emphasis on increasing surface hydrophobicity alone. Lastly, the permeability/wetting resistance tradeoff in MD is considered with respect to membrane modifications that improve resistance to scaling- and surfactant-induced wetting.

#### 2. Materials and Methods

#### 2.1. Membranes and membrane modification

Two commercial flat-sheet membranes were used as substrates: an expanded polytetrafluoroethylene (PTFE) membrane (Parker Performance Materials, Lees Summit, MO) and a cellulose acetate (CA) membrane (Sterlitech, Kent, WA). The PTFE membrane is hydrophobic and symmetric, with a pore size of  $0.2 \, \mu m$ , a bulk porosity of  $84 \pm 0.5\%$ , and a thickness of  $67 \pm 5 \, \mu m$ . The CA membrane is hydrophilic and symmetric, with a pore size of  $0.2 \, \mu m$ , a bulk porosity of  $55 \pm 1\%$ , and a thickness of  $83 \pm 2 \, \mu m$ . Bulk porosity was measured according to the gravimetric method.<sup>7</sup> Reported values represent an average of measurements for three samples of each membrane. For uncoated membranes, polymer densities of  $2.2 \, \mu m$  and  $1.3 \, g/cm^3$  were used for PTFE and CA. For coated membranes, average polymer densities were assumed to be similar to those of the corresponding substrates (due to the relatively small amount of coating added). Membrane thicknesses were measured using a micrometer (MDC-1 PX, Mitutoyo, Kawasaki, Japan) with an accuracy of  $\pm 1 \, \mu m$ . Reported values represent an average of at least eight measurements at different locations on each sample. The uncoated PTFE membrane, which has performed well during long-term operation in previous studies (i.e., Gustafson et al.<sup>12</sup>, McGaughey et al.<sup>81</sup>), was tested in MD experiments for comparison with the coated membranes. The uncoated CA membrane was not used for comparison because the pores would readily wet under MD conditions.

Both substrates were coated with the crosslinked fluoropolymer P(PFDA-co-EGDA). Crosslinking increases the coating durability.<sup>62</sup> The coatings were fabricated using 1H,1H,2H,2H-perfluorodecyl acrylate (PFDA) monomer (SynQuest, Alachua, FL), ethylene glycol diacrylate (EGDA) crosslinker (Polysciences, Inc., Warrington, PA), and di-tert-butyl peroxide (TBPO) (98%) (Sigma-Aldrich, St. Louis, MO) initiator; all were used as received without further purification.

The P(PFDA-co-EGDA) coating was deposited onto the substrates using a custom designed iCVD reactor (GVD Corporation, Cambridge, MA) that is 250 mm in diameter and 48 mm in height. For each deposition, a 6 x 6 cm substrate coupon was taped on the reactor stage that was cooled to 30 °C via a recirculating chiller. The PFDA and EGDA monomer jars were heated to 45 and 30 °C, respectively; the monomer lines were heated to 15 °C above the jar temperatures to provide flow rates of 0.1 sccm for each. The TBPO initiator jar was held at room temperature and a mass flow controller (MKS 1479A, Andover, MA) was used to provide an initiator flow rate of 0.3 sccm. The filament array (80% Ni, 20% Cr) (Omega Engineering, Stamford, CT) was resistively heated to 250 °C. A pressure transducer (Baratron capacitance manometer 622A01TDE, MKS) was used to measure the reactor pressure and an automated butterfly valve was used to maintain a reactor pressure of 90 milliTorr, which resulted in a deposition rate of 30 nm/min. Deposition rate was monitored on a reference silicon wafer in real-time using an *in-situ* laser interferometer (Helium-Neon, 633 nm) (Industrial Fiber Optics, Tempe, AZ). Coatings were deposited to a final thickness of 400 nm.

#### 2.2. Characterization

#### 2.2.1. Surface characterization

Contact angle ( $\theta$ ) was measured using a goniometer (Model 260, ramé-hart, Succasunna, NJ) and the sessile drop method with 5-µL droplets. Reported values represent an average of at least five measurements on the sample surface. Surface morphology was characterized using a field-emission scanning electron microscope (JSM-7001, Jeol USA, Huntington Beach CA). Samples were sputter-coated for 60 s prior to imaging. ImageJ software (version 1.49, National Institutes of Health, Bethesda MD) was used to determine surface porosity ( $\epsilon$ ) and surface pore size ( $d_p$ ). Reported values represent averaged data from SEM images of three arbitrary areas of both sides of each membrane. Surface pore size distributions were determined as histograms of surface pore sizes normalized by probability density using MATLAB software (version R2018b, MathWorks, Natick, MA); three histograms (corresponding to the three arbitrary areas imaged) were obtained for each surface. For all distributions, the skewness, or asymmetry of the distribution, was also calculated using MATLAB software. Positive skewness of a distribution indicates that the distribution is weighted towards smaller values and negative skewness indicates that the distribution is weighted towards larger values.

Surface roughness was analyzed using an atomic force microscope (Innova, Bruker, Billerica MA). Gwyddion software (version 2.47, Czech Metrology Institute, Brno, Czech Republic) was used to calculate surface roughness. Reported values represent averaged data from scans of three arbitrary areas of each surface. Membrane surface elemental compositions were analyzed using x-ray photoelectron spectroscopy (XPS) (Axis Ultra DLD, Kratos Analytical, Manchester, UK) with a monochromatic Al K-alpha x-ray source. Survey spectra were collected over a binding energy range of 0 to 900 eV with a step size of 1 eV. The XPS data were analyzed using CasaXPS software (Casa Software, Teignmouth, UK).

 $\Delta G_M^*$  was calculated according to: 17,48

$$\Delta G_M^* = \Delta G_{homogeneous}^* \left(\frac{1}{4}\right) (1 + \cos\theta) (1 - \cos\theta)^2 \left(1 - \epsilon \frac{(1 + \cos\theta)^2}{(1 - \cos\theta)^2}\right)^3 \tag{3}$$

LEP was calculated according to the Kim and Harriott<sup>46</sup> model in equation (2), where  $\theta$  is the intrinsic advancing contact angle. For the PTFE membrane, intrinsic advancing contact angle values reported by Morra et al.<sup>63</sup> were used; for the coated membranes, intrinsic advancing contact angle values were measured by coating P(PFDA-co-EGDA) on a silicon wafer and measuring the advancing contact angle. R/r was determined from atomic force microscopy (AFM) results and Gwyddion software according to the method validated by Guillen-Burrieza et al.<sup>45</sup> Surface tension was taken as that of deionized water at 25 °C.

Theoretical minimum LEP values were calculated using the average maximum surface pore radius of each membrane. LEP distributions were determined using all surface pore sizes (i.e., the surface pore size distribution) from each area. LEP distributions were presented as histograms of LEP values normalized by probability density. LEP distributions were determined for three arbitrary areas of each membrane surface.

Experimental LEP values were measured by gradually increasing the applied pressure on a saline solution in contact with the feed side of a membrane sample placed in a pressure cell (Advantec MFS, Dublin, CA), with deionized water on the distillate side. The experimental LEP was determined as the minimum pressure at which an increase in distillate conductivity was detected.

## 2.2.2. Performance characterization

Membrane performance was tested using a custom-built, bench-scale MD system (Supporting Information, Figure S1) and a custom-made acrylic module with an active area of 20 cm<sup>2</sup>. 65-mm mesh spacers (Sterlitech) were placed in the feed and distillate channels. For all experiments, the top side of the membranes faced the feed solution.

Feed and distillate solutions were recirculated counter-currently at constant flow rates of 0.76 L/min using a peristaltic pump (Masterflex, Cole Parmer, Vernon Hills, IL) on the feed side and a gear pump (Micropump, Vancouver, WA) on the distillate side. Flow rates were monitored using manual flow meters (Omega Engineering). Feed stream temperatures were controlled using a recirculating heater and distillate stream temperatures were controlled using a recirculating chiller (Cole Parmer). Feed and distillate stream temperatures and pressures were measured at the module inlet and outlet using in-line resistance temperature detectors (Omega Engineering) and pressure probes (feed-side, Omega Engineering; distillate-side, Cole-Parmer). Feed and distillate stream conductivities were continuously monitored using in-line conductivity probes (Cole-Parmer). Non-metallic or titanium components were used on the feed side to prevent corrosion. Data were recorded at 30-second intervals using a custom data acquisition and control program developed in LabView (National Instruments, Austin, TX). Distillate overflow was continuously monitored with a digital balance (Ohaus, Parsippany, NJ) and flux ( $I_w$  in kg/m²s) was calculated as

$$J_w = \frac{m_d}{a_m \Delta t} \tag{4}$$

where  $m_d$  is the change in distillate mass (kg) during time interval  $\Delta t$  (s) and  $a_m$  is the membrane area (m<sup>2</sup>). Rejection (R, unitless) was calculated according to

$$R = 1 - \frac{C_{D,t_2}V_{D,t_2} - C_{D,t_1}V_{D,t_1}}{C_{F,t_2}V_{D,t_2} - C_{F,t_1}V_{D,t_1}}$$
(5)

where  $C_{D,t}$  is distillate concentration (mol/L NaCl) at time t,  $V_{D,t}$  is distillate volume at time t (m³), and  $C_{F,t}$  is feed concentration (mol/L NaCl) at time t.8

## Scaling experiments

For experiments evaluating scaling of the membrane, 5-M NaCl (VWR) was used as the feed solution. The bench-scale system was operated in batch mode (i.e., without replenishment or dilution of feed solution) and experiments were terminated when distillate conductivity exceeded 200  $\mu$ S/cm or after 12 h. Operating temperatures and pressures were taken after temperatures stabilized (i.e., after 1 h operation) until the end of each experiment. Average operating feed and distillate stream temperatures were 52 ± 1 and 17 ± 0.8 °C. Average feed and distillate stream pressures were 13 ± 1 and 12 ± 0.7 kPa; thus, the impact of hydraulic pressure difference on wetting and salt flux were assumed negligible.

## Surfactant experiments

For experiments evaluating surfactant fouling of the membrane, 200 ppm anionic surfactant (Triton X-100, Sigma-Aldrich) in 1 M NaCl was used as the feed solution. The bench-scale system was operated with constant feed solution concentration for 5 h; if wetting did not occur by that time, the system was switched to batch mode to increase surfactant concentration. Experiments were terminated when distillate conductivity exceeded 200  $\mu$ S/cm or after 25 h. Operating temperatures were taken after temperatures stabilized (i.e., after 1 h of operation) until the end of each experiment. Average feed and distillate stream temperatures were 52 ± 0.7 and 18 ± 0.9 °C. Average feed and distillate stream pressures were 12 ± 0.8 and 12 ± 0.9 kPa; thus, the impact of hydraulic pressure difference on wetting and salt flux were assumed negligible.

In all cases, statistical significances were evaluated by performing two-sided t-tests at a significance level  $(\alpha)$  of 0.05. Unequal variances were assumed.

#### 3. Results and Discussion

## 3.1. Surface characteristics of uncoated and coated membranes

Surface roughness and contact angle values for both sides of the uncoated and coated membranes are shown in Table 1. For both uncoated and coated membranes, surface roughness values are greater for the CA membranes than the PTFE membranes; the differences in surface roughness between the CA and PTFE membranes are statistically significant (as confirmed by t-tests with  $\alpha = 0.05$ ). While the

standard deviations shown in Table 1 are relatively high, indicating spatial variability, the coefficients of variation (i.e., the ratio of the standard deviation to the mean; not shown in Table 1) are comparable to those of previous studies (e.g., Koyuncu et al.<sup>64</sup>).

**Table 1.** Root-mean-square 2-D surface roughness and contact angle values of uncoated and coated membranes. The ± values in parentheses represent standard deviations.

	Surface rou	ghness (nm)	Contact angle (°)		
Membrane	Тор	Bottom	Тор	Bottom	
CA	468 (±156)	313 (±101)	0	0	
PTFE	214 (±49)	99 (±3)	149 (±3)	145 (±2)	
Coated CA	471 (±152)	438 (±99)	157 (±5)	158 (±8)	
Coated PTFE	222 (±15)	115 (±33)	143 (±3)	145 (±7)	

For all membranes, top and bottom contact angle measurements are similar (Table 1). The uncoated CA membrane has a contact angle of zero on each side since water droplets are readily absorbed by the hydrophilic membrane and a static sessile drop contact angle could not be measured. The generally greater contact angles on the coated CA membranes compared to the coated PTFE membranes, despite both membranes having the same coating, are likely due to the inherently rougher surface of the CA membrane, as greater surface roughness results in higher contact angles on hydrophobic surfaces. Differences in contact angle between the CA and PTFE membranes are statistically significant (as confirmed by t-tests with  $\alpha$  = 0.05).

Representative SEM images for both sides of the uncoated and coated membranes are shown in Figure 1. Surface porosity and surface pore size values for all membranes are shown in Table 2.

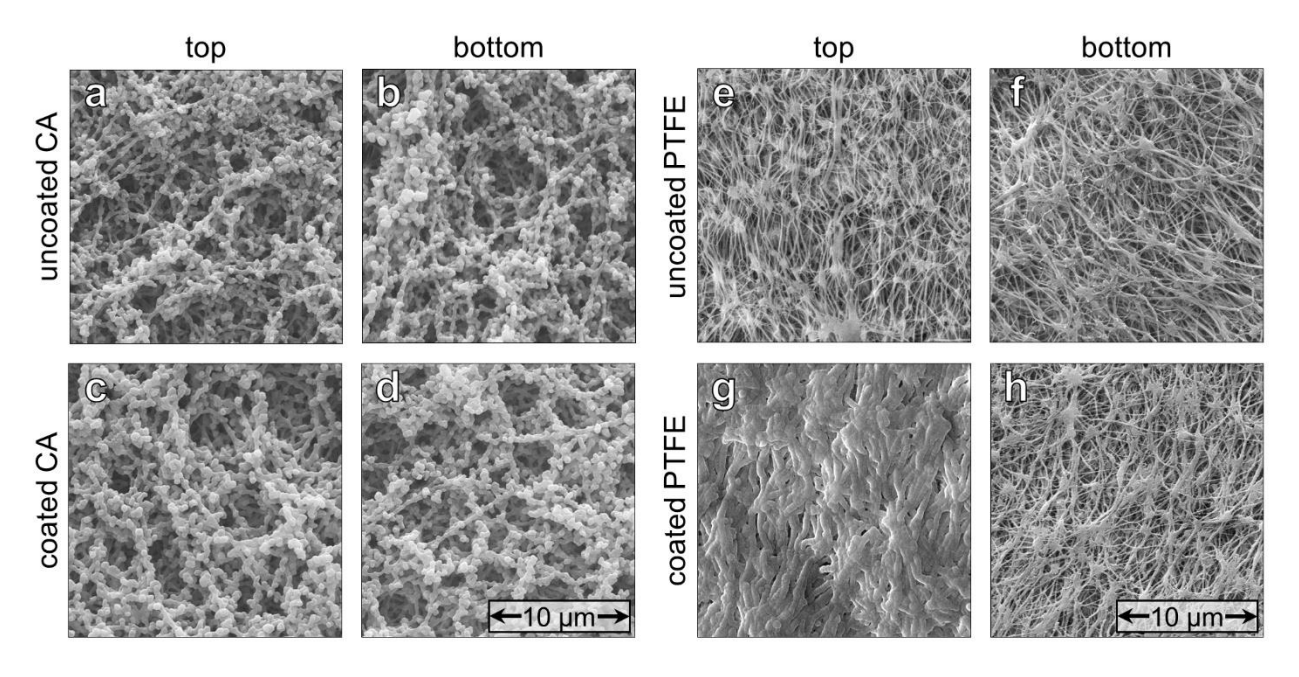


**Figure 1.** Representative SEM images of **a**) top and **b**) bottom of the uncoated CA membrane; **c**) top and **d**) bottom of the coated CA membrane; **e**) top and **f**) bottom of the uncoated PTFE membrane; and **g**) top and **h**) bottom of the coated PTFE membrane. All images taken at x 4,000 magnification.

**Table 2.** Surface pore parameters of the uncoated and coated membranes. For the uncoated membranes, parameters are shown as an average of both sides of the membranes since they are symmetric. For the coated membranes, parameters are shown separately for each side due to the nature of the iCVD coating technique. The ± values in parentheses represent standard deviations.

Membrane	Surface porosity (%)		Average surface pore size (nm)		Maximum surface pore size (µm)		
CA	27 (±8)		159 (±38)		3.2 (±0.9)		
PTFE	21 (±2)		133 (±5)		1.3 (±0.1)		
	Тор	Bottom	Тор	Bottom	Тор	Bottom	
Coated CA	21.0 (±4)	25.8 (±3)	132 (±4)	132 (±5)	3.4 (±1)	2.8 (±0.4)	
Coated PTFE	3.5 (±2)	26 (±1)	64 (±5)	125 (±4)	1.4 (±0.3)	1.5 (±0.2)	

Visual comparison of the top and bottom sides of the uncoated CA membrane (i.e., comparison of Figures 1a and b), shows similar morphology on both sides of the membrane. Comparison of the top and bottom sides of the coated CA membranes (i.e., comparison of Figures 1c and d) also shows similar morphology. Data in Table 2 show that the coating process did not significantly change the surface porosity, average surface pore size, or maximum surface pore size of either side of the CA membrane, as confirmed by t-tests with  $\alpha = 0.05$ . The lack of significant visual or measured differences between the top and bottom sides of the coated CA membrane indicates that the substrate was evenly coated from the top to the bottom; in other words, the P(PFDA-co-EGDA) coating appeared to be conformal in the z-direction.

Similar to the uncoated CA membrane, visual comparison of Figures 1e and f shows similar morphology on both sides of the uncoated PTFE membrane. However, for the coated PTFE membrane, it can be seen on the top side (Figure 1g) that the fibrils and nodes have increased thicknesses, whereas on the bottom side (Figure 1h) they appear relatively similar to the uncoated PTFE membrane. Thus, the P(PFDA-co-EGDA) coating thickness appeared to be greater on the top side than on the bottom side, suggesting non-conformality in the z-direction. Data in Table 2 support the visual observations: the top-side average surface pore size and porosity decreased significantly after coating, but the bottom-side porosity and average pore size did not (as confirmed by t-tests with  $\alpha=0.05$ ). The maximum surface pore size did not change significantly on either side. Pore size distribution results are shown in the Supporting Information (Section S2.2). For the coated membranes, bulk porosities were approximately 42 ± 3% and 66 ± 1%, respectively. As expected, the bulk porosities of the membranes decreased after they were coated. For all membranes, surface porosity and average pore size values are lower than the corresponding bulk values likely due to larger voids present in the bulk of the membrane (e.g., Supporting Information Figure S2).

Elemental composition results from XPS analysis of the uncoated and coated membranes are shown in Table 3. For the uncoated CA membrane, only carbon and oxygen were detected, as expected. For the coated CA membrane, fluorine was detected, indicating the presence of the P(PFDA-co-EGDA) coating; XPS results were similar on both sides of the coated CA membrane, indicating that the coating is conformal. For the uncoated PTFE membrane, carbon, oxygen, fluorine, and silicon were detected. On the top side of the coated PTFE membrane, a higher fluorine percentage and lack of silicon indicate that the coating thickness exceeded the XPS penetration depth of 5 nm; on the bottom side, the appearance of the silicon peak indicates that the penetration depth exceeded the coating thickness (i.e., the coating is less than 5 nm thick). These results indicate that the coating on the PTFE membrane is thicker on the top than on the bottom (i.e., the coating is nonconformal). Also, less fluorine was detected on the bottom side of the coated PTFE membrane than on the top side, which may indicate a compositional gradient in the copolymer coating in the z-direction (i.e., a higher PFDA:EGDA ratio on the top side than on the bottom side). The XPS results are consistent with the SEM results (Figure 1), pore parameter results (Table 2), and pore size distribution results (Supporting Information, Figure S3).

**Table 3.** Percent composition results from XPS analysis of uncoated and coated membranes. For uncoated membranes, results are shown for a single side representing the symmetric material. For the coated membranes, results are shown separately for each side due to the nature of the iCVD coating technique.

		Percent composition (%)							
Membrane	Ca	<u>Carbon</u>		<u>Oxygen</u>		<u>Fluorine</u>		Silicon	
CA		52		48		-*		_*	
PTFE		50	21		24		5		
	Тор	Bottom	Тор	Bottom	Тор	Bottom	Тор	Bottom	
Coated CA	41	43	6	6	53	50	_*	_*	
Coated PTFE	32	59	7.5	26	60	13	_*	2.6	

<sup>\* -</sup> indicates element was not detected

As discussed in Section 1.2, conformality in iCVD is affected by the fractional saturation of monomer in the reactor and by the aspect ratio of the substrate pores. $^{20,58}$  In the present study, an identical coating material and identical operating parameters (including the fractional monomer saturation) were used. Regarding aspect ratio: due to the greater thickness of the CA substrate (83 ± 2 µm) than of the PTFE substrate (67 ± 5 µm), the aspect ratio of the CA substrate is slightly higher, which was expected to result in less conformal coatings compared to the PTFE substrate. However, the opposite was observed: the CA substrate coating is more conformal than the PTFE substrate coating. Therefore, it appears that substrate surface energy may affect conformality. The monomer appears to have had greater affinity for the high-surface-energy (~40 mN/m<sup>65</sup>) CA substrate than the low-surface-energy (~21 mN/m<sup>66</sup>) PTFE substrate and, therefore, adsorbed more uniformly on the CA substrate.

## 3.2. Liquid entry pressure

Figure 2 shows the theoretical minimum LEP and LEP distribution for the top (feed) side of the membranes. Despite the higher contact angle of the coated CA membrane compared to the coated PTFE membrane (Table 1), the coated CA membrane has a lower minimum LEP due to its higher maximum pore size (as calculated by the Young-Laplace and Kim-Harriott LEP models and shown in Table 2). Based on minimum LEP results, the coated CA membrane is more likely to wet than the uncoated PTFE and coated PTFE membranes.

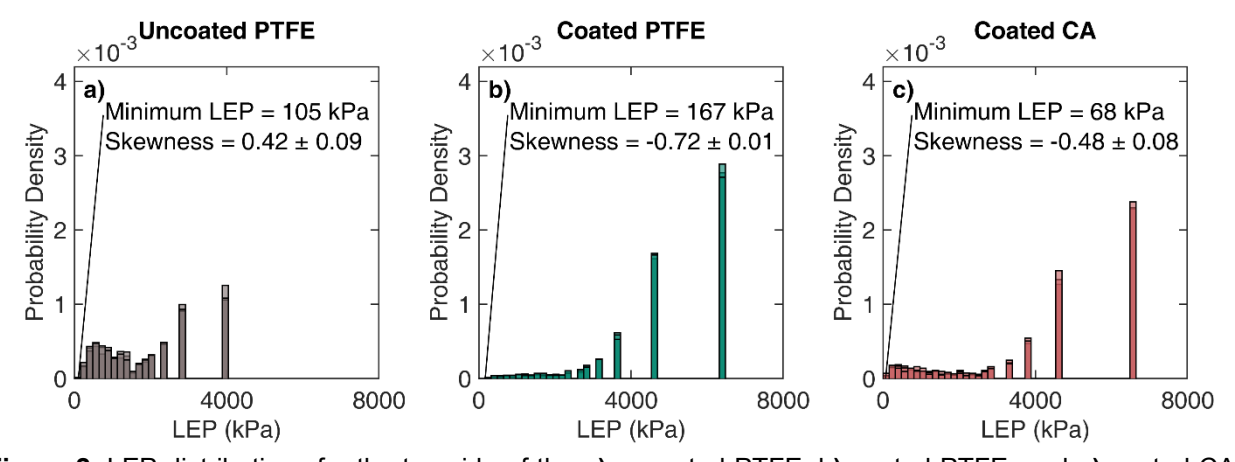


**Figure 2**. LEP distributions for the top side of the **a)** uncoated PTFE, **b)** coated PTFE, and **c)** coated CA membranes. For each membrane, results are shown as three overlaid histograms normalized by probability density, as discussed in Section 2.

To verify the theoretical LEP results, the experimental LEP was measured for the uncoated PTFE membrane. Based on four samples, the experimental minimum LEP was  $102 \pm 7$  kPa; this value agrees well with theoretical results (Figure 2a). As experimental LEPs of commercial membranes used for MD are typically between 100 and 440 kPa; the values in the current study are at the lower end of this range.

For LEP measurements of the uncoated PTFE membrane, the experimental minimum LEP was determined when a slight increase in distillate conductivity occurred. The rate of change of distillate conductivity

increased as pressure was increased further. At approximately 345 kPa, which agrees with previously reported values,<sup>3</sup> more significant salt passage and distillate flow (as may be detectable in an MD system) occurred. This higher LEP value likely represents wetting of multiple pores. As discussed in Section 1.1, in LEP systems - and in real MD systems - wetting of multiple pores likely occurs before wetting is detected. Therefore, the theoretical minimum LEP (representing wetting of the largest pore) may not be of practical importance.

Because LEP is dependent on pore size and membranes are characterized by a pore size distribution, expressing LEP as a distribution will provide greater ability to characterize wetting resistance. The skewness of the LEP distributions, which results directly from pore size distribution skewness (Figure S3), can be used to indicate membrane wetting resistance. The uncoated PTFE membrane (Figure 2a) has a positively skewed LEP distribution and both coated membranes have negatively skewed LEP distributions (Figures 2b and c). Negatively skewed LEP distributions indicate that the distribution is weighted toward higher LEPs or that there is a greater frequency of surface pores with high LEP, which may indicate higher overall wetting resistance. For all membranes, differences in skewness were statistically significant at  $\alpha$  = 0.05. The greater likelihood of the uncoated PTFE membrane to wet than either of the coated membranes is in contrast with the minimum LEP results (Figure 2), which suggest that the coated CA membrane is most likely to wet.

## 3.3. Scaling-induced wetting performance

Performance results under scaling-induced wetting conditions are shown in Figure 3. In terms of water flux, both coated membranes had lower fluxes than the uncoated PTFE membrane but operated stably (Figure 3a). The lower water flux observed for the coated PTFE membrane relative to the uncoated PTFE membrane is likely in large part due to its lower bulk and surface porosity. The lower water flux for the coated CA membrane is likely due to its lower bulk porosity and greater thickness. For the uncoated PTFE membrane, distillate conductivity sharply increased (Figure 3b) and conductivity rejection decreased (Figure 3c) (i.e., wetting occurred) after approximately 1.3 h operation. Wetting was likely due to concentration polarization resulting in exceedance of the saturation concentration of NaCl (5.5 M at 53 °C) and subsequent scaling. Scaling at the membrane surface could then lead to intrapore crystal growth, which provides a hydrophilic surface that facilitates liquid entry into the pores.

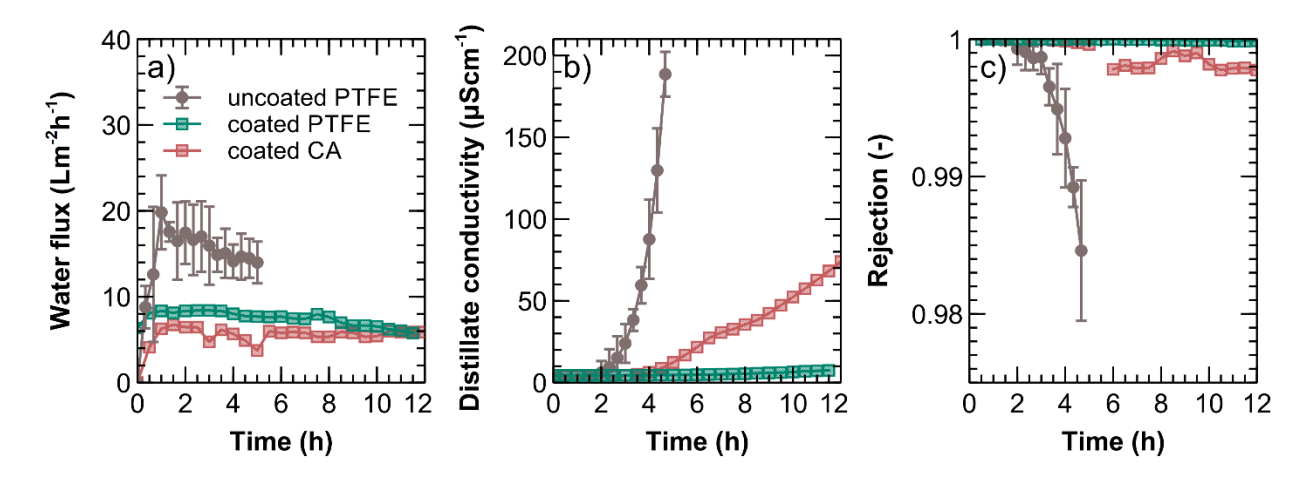


**Figure 3.** Performance of the uncoated PTFE, coated PTFE, and coated CA membranes with 5 M NaCl feed solution in terms of **a**) water flux, **b**) distillate conductivity, and **c**) solute rejection.

Both coated membranes experienced delayed wetting and salt passage relative to the uncoated PTFE membrane.  $\Delta G_{M,NaCl}^*$  results for the uncoated PTFE and coated membranes are shown in Table 4. The slightly higher  $\Delta G_{M,NaCl}^*$  of the coated CA membrane compared to the uncoated PTFE membrane (Table 4) may have delayed surface nucleation, and hence, scaling and wetting; the difference is statistically significant at  $\alpha = 0.05$ . However, after ~4.3 h operation, wetting did occur for the coated CA membrane (Figures 3b and c). Heterogeneous nucleation and/or deposition of crystals nucleated in bulk solution may have resulted in surface scaling and led to wetting. Notably,  $\Delta G_{M,NaCl}^*$  for the coated CA membrane is near the theoretical maximum  $\Delta G_{M,NaCl}^*$  (455 MJ/mol) obtained at a contact angle of 180° and a surface porosity of zero; thus, additional increases in contact angle (or reductions in surface porosity) would result in minimal increases in  $\Delta G_{M,NaCl}^*$ .

**Table 4.**  $\Delta G_{M,NaCl}^*$  of the uncoated PTFE, coated PTFE, and coated CA membranes; results are for 5 M NaCl at 25 °C.

Membrane	$\Delta G_{M,NaCl}^*$ (MJ/mol)
PTFE	447
Coated PTFE	445
Coated CA	454

The coated PTFE membrane did not wet over the duration of the experiment (Figures 3b and c). Interestingly, this was the case even though the coated PTFE membrane has a similar  $\Delta G_{M,NaCl}^*$  to the uncoated PTFE membrane (Table 4). Gryta<sup>23</sup> suggests that small pore size (relative to crystal size) can restrict intrapore crystal growth. However, size exclusion likely will not prevent all intrapore scaling. For example, for sodium chloride, critical nucleus sizes as small as ~10 molecules have been reported;<sup>47</sup> these could form in small pores. However, this mechanism of intrapore nucleation can only occur in already-

wetted pores. We suggest that the higher LEP of the coated PTFE membrane compared to the uncoated PTFE membrane (Figure 2) may prevent partial wetting and, therefore, intrapore nucleation and crystal growth – regardless of size exclusion effects. Notably, the LEP of the uncoated PTFE membrane is high because of its small average surface pore size (Table 2); this is not due to size exclusion but because smaller pores mean that the curvature of the meniscus of the penetrating solution is greater, which increases the Laplace pressure of the meniscus<sup>67</sup> and, therefore, the LEP. By preventing wetting, the higher LEP at the entrance of smaller pores may prevent intrapore nucleation and crystal growth regardless of size exclusion effects. Surface roughness effects may also contribute; as noted by Meng et al.<sup>39</sup>, higher surface roughness may increase the number of available nucleation sites on a membrane. The coated CA membrane is more rough than the coated PTFE membrane (Table 1).

To more broadly examine the effectiveness of increased hydrophobicity and  $\Delta G_{M,NaCl}^*$  as a strategy to reduce scaling-induced wetting, a sensitivity analysis of  $\Delta G_{M,NaCl}^*$  was performed (Figure 4). Ranges of contact angle (90 to 180°) and surface porosity (0 to 1) were selected to bracket the membranes used in this study. It can be seen that above a contact angle of 140°,  $\Delta G_{M,NaCl}^*$  approaches a constant value. Therefore, increasing hydrophobicity to increase  $\Delta G_{M,NaCl}^*$  of a membrane is inherently limited as a scaling mitigation strategy.

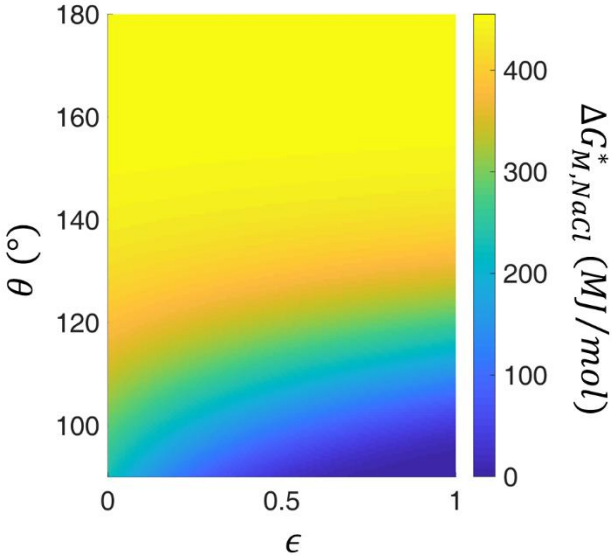


**Figure 4.** Sensitivity analysis of  $\Delta G_{M,NaCl}^*$  for heterogeneous NaCl nucleation from 5 M solution at 25°C to contact angle ( $\theta$ ) and surface porosity ( $\epsilon$ ).

## 3.4. Surfactant-induced wetting performance

Performance results under surfactant-induced wetting conditions are shown in Figure 5. Similar to scaling-induced wetting conditions, both coated membranes had lower water fluxes than the uncoated PTFE membrane but operated stably (Figure 5a). Also similar to the scaling-induced wetting conditions, the lower

water flux observed for the coated PTFE membrane is likely due to its lower porosity relative to the uncoated PTFE membrane, and the lower water flux observed for the coated CA membrane is likely due to its lower bulk porosity and greater thickness compared to the uncoated PTFE membrane. For the uncoated PTFE membrane, wetting occurred after approximately 1.3 h operation (Figures 5b and c), likely due to reduced surface tension at the membrane surface resulting from concentration polarization.<sup>14</sup>

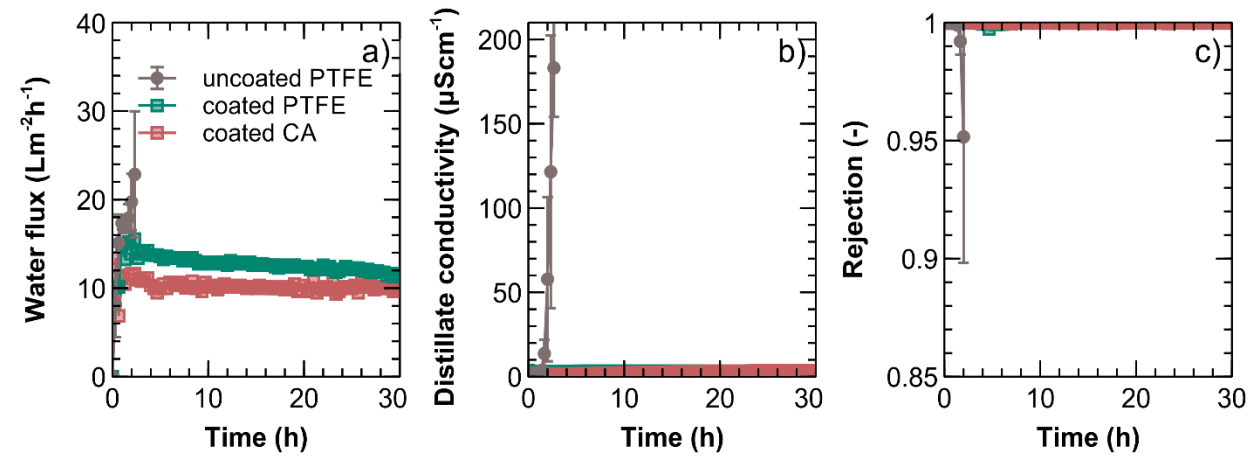


**Figure 5.** Performance of uncoated PTFE, coated PTFE, and coated CA membranes with 200 ppm surfactant in 1 M NaCl feed solution in terms of **a**) water flux, **b**) distillate conductivity, and **c**) solute rejection.

No wetting was observed for either coated membrane (Figures 5b and c). Unlike for scaling-induced wetting conditions, the difference in surface pore size and porosity between the coated membranes (Table 2) did not correspond to a difference in surfactant-induced wetting resistance. Instead, the more hydrophobic coated CA membrane and the smaller surface pore size/porosity coated PTFE membrane had equivalent wetting resistance over the duration tested.

Also, the difference in minimum LEP values for the coated membranes (Figure 2) did not correspond to a difference in wetting resistance. Instead, surfactant-induced wetting results corresponded to expectations based on LEP distributions: while the uncoated PTFE membrane had a positively skewed LEP distribution (Figure 2a), both coated membranes had negatively skewed LEP distributions (Figures 2b and c). In other words, both coated membranes had fewer large surface pores with low LEPs; this may prevent measurable wetting. Additionally, large surface pores located adjacent to each other, which can facilitate wetting, <sup>13</sup> may be less likely in the coated membranes due to the low frequency of large surface pores.

To more broadly examine the impact of pore size and contact angle on wetting resistance, a sensitivity analysis of LEP to contact angle and pore diameter was performed (Figure 6). The contact angle range (90 to 180°) was selected to represent the full range of hydrophobic membranes; the pore size range (0.05 to 0.3 µm) was selected to represent average pore sizes typically used for MD membranes. Figure 6 illustrates

how LEP generally increases with increasing contact angle (and, therefore, with decreasing surface energy) and how LEP generally increases with decreasing pore size, as defined by the Young-Laplace model. Small pore diameters are necessary to access the highest LEP values because LEP is inversely proportional to pore diameter. Despite this, as discussed in Section 1, the majority of MD membrane modification strategies have focused on increasing membrane surface hydrophobicity to increase wetting resistance. This is likely because reducing porosity and pore size can negatively affect water flux.<sup>3,43</sup>

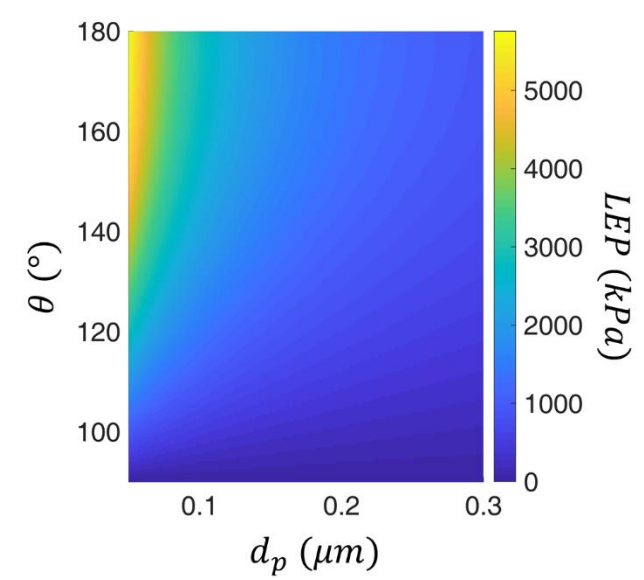


**Figure 6.** Sensitivity analysis of LEP to contact angle  $(\theta)$  and pore diameter  $(d_v)$ .

#### 4. Conclusions and Implications

The CA membrane was coated conformally and became symmetric and superhydrophobic. The PTFE membrane was coated nonconformally and became asymmetric, with smaller pore size and lower porosity on the top than on the bottom surface. The difference in conformality may be linked to substrate surface energy: for the CA membrane, higher substrate surface energy may have resulted in greater affinity for the monomer, leading to more uniform monomer concentration within pores and therefore formation of a more conformal polymer layer. In MD performance testing, both coated membranes outperformed the uncoated PTFE membrane. However, key differences between the performances of the coated membranes were observed.

Under scaling-induced wetting conditions, the coated PTFE membrane, due to its smaller surface pore size and porosity, had higher wetting resistance than the coated CA membrane, despite the higher  $\Delta G_{M,Nacl}^*$  of the coated CA membrane. While increasing surface hydrophobicity can delay surface nucleation, surface scaling can also occur by deposition of salt crystals formed elsewhere. Prevention of intrapore scaling may be necessary to prevent wetting in longer-term operation. Small surface pore sizes and/or porosity may more effectively prevent intrapore scaling due to high LEP at pore entrances, which may prevent partial wetting and, therefore, intrapore nucleation. Under surfactant-induced wetting conditions, the coated membranes performed equally well. The reduced surface pore size and porosity of the coated PTFE membrane were as effective as the increased surface hydrophobicity of the coated CA membrane. Also, wetting resistances were better predicted by LEP distributions than by minimum LEP values. When LEP distributions are (negatively) skewed towards higher LEP values, small pores with high LEP are greater in number and significant, measurable salt passage may be prevented.

The results of this study challenge past emphasis on increasing surface hydrophobicity alone to improve the wetting resistance of MD membranes. Reducing surface pore size and porosity can be more effective than increasing surface hydrophobicity and may be a viable strategy to impart high wetting resistance without relying on perfluorinated coating materials. However, importantly, reducing surface porosity and pore size can negatively impact flux, resulting in a permeability/wetting resistance tradeoff in MD – especially for high-salinity applications. If key properties are optimized (e.g., by maximizing pore density and/or by minimizing the thickness of the small-pore-size/porosity surface layer or membrane), it may be possible to overcome the permeability/wetting resistance tradeoff. When coating membranes to achieve high wetting resistance without sacrificing water flux, coating conformality could be minimized.<sup>20</sup> It has also been suggested that permeability can be maintained by increasing the pore density and/or by reducing the thickness of the small-pore-size surface layer,<sup>20</sup> but the effect on wetting resistance for challenging solutions has not yet been considered. Thin, self-standing, dense hydrophobic membranes (e.g., Mejia Mendez et al.<sup>68</sup>) and hydrophobic membranes with thin, low porosity surface layers (e.g., Shaulsky et al.<sup>69</sup> and Nejati et al.<sup>70</sup>) could overcome the permeability/wetting resistance tradeoff in MD; however, these membranes have not yet been tested under wetting conditions.

#### **Associated Content**

#### **Supporting Information**

Schematic of bench-scale MD system used for performance characterization, cross-sectional SEM results, surface pore size distributions of uncoated and coated membranes, and SEM and energy dispersive x-ray spectroscopy analysis results for used membranes after scaling- and surfactant-induced wetting performance tests.

## Acknowledgements

This material is based on work supported by the National Science Foundation under grant number 1820389. We would also like to acknowledge funding support from an American Membrane Technology Association and Affordable Desalination Coalition fellowship awarded to A. L. McGaughey. SEM and XPS data were collected at the University of Southern California Core Center of Excellence in Nano Imaging (CNI) and AFM data was collected at the University of Southern California Center of Excellence in NanoBiophysics.

#### References

- 1. Deshmukh, A.; Boo, C.; Karanikola, V.; Lin, S.; Straub, A. P.; Tong, T.; Warsinger, D. M.; Elimelech, M., Membrane distillation at the water-energy nexus: limits, opportunities, and challenges. *Energy & Environmental Science* **2018**, *11* (5), 1177-1196.
- 2. Martinetti, C. R.; Childress, A. E.; Cath, T. Y., High recovery of concentrated RO brines using forward osmosis and membrane distillation. *Journal of Membrane Science* **2009**, *331* (1), 31-39.
- 3. Rao, G.; Hiibel, S. R.; Childress, A. E., Simplified flux prediction in direct-contact membrane distillation using a membrane structural parameter. *Desalination* **2014**, *351*, 151-162.
- 4. Cath, T. Y.; Adams, V. D.; Childress, A. E., Experimental study of desalination using direct contact membrane distillation: a new approach to flux enhancement. *Journal of Membrane Science* **2004**, *228* (1), 5-16.
- 5. Salls, K. A.; Won, D.; Kolodziej, E. P.; Childress, A. E.; Hiibel, S. R., Evaluation of semi-volatile contaminant transport in a novel, gas-tight direct contact membrane distillation system. *Desalination* **2018**, 427. 35-41.
- 6. Cath, T. Y.; Adams, D.; Childress, A. E., Membrane contactor processes for wastewater reclamation in space: II. Combined direct osmosis, osmotic distillation, and membrane distillation for treatment of metabolic wastewater. *Journal of Membrane Science* **2005**, *257* (1), 111-119.
- 7. Rao, G.; Hiibel, S. R.; Achilli, A.; Childress, A. E., Factors contributing to flux improvement in vacuum-enhanced direct contact membrane distillation. *Desalination* **2015**, *367*, 197-205.
- 8. Morrow, C. P.; Furtaw, N. M.; Murphy, J. R.; Achilli, A.; Marchand, E. A.; Hiibel, S. R.; Childress, A. E., Integrating an aerobic/anoxic osmotic membrane bioreactor with membrane distillation for potable reuse. *Desalination* **2018**, *432*, 46-54.
- 9. Gustafson, R. D.; Hiibel, S. R.; Childress, A. E., Membrane distillation driven by intermittent and variable-temperature waste heat: System arrangements for water production and heat storage. *Desalination* **2018**, *448*, 49-59.
- 10. Suárez, F.; Ruskowitz, J. A.; Tyler, S. W.; Childress, A. E., Renewable water: direct contact membrane distillation coupled with solar ponds. *Applied energy* **2015**, *158*, 532-539.
- 11. Suárez, F.; Tyler, S. W.; Childress, A. E., A theoretical study of a direct contact membrane distillation system coupled to a salt-gradient solar pond for terminal lakes reclamation. *Water Research* **2010**, *44* (15), 4601-4615.
- 12. Gustafson, R. D.; McGaughey, A. L.; Ding, W.; McVety, S. C.; Childress, A. E., Morphological changes and creep recovery behavior of expanded polytetrafluoroethylene (ePTFE) membranes used for membrane distillation. *Journal of Membrane Science* **2019**, *584*, 236-245.
- 13. Warsinger, D. M.; Swaminathan, J.; Guillen-Burrieza, E.; Arafat, H. A.; Lienhard V, J. H., Scaling and fouling in membrane distillation for desalination applications: A review. *Desalination* **2015**, *356*, 294-313.
- 14. Wang, Z.; Chen, Y.; Sun, X.; Duddu, R.; Lin, S., Mechanism of pore wetting in membrane distillation with alcohol vs. surfactant. *Journal of Membrane Science* **2018**, *559*, 183-195.
- 15. Rezaei, M.; Warsinger, D. M.; Lienhard V, J. H.; Duke, M. C.; Matsuura, T.; Samhaber, W. M., Wetting phenomena in membrane distillation: Mechanisms, reversal, and prevention. *Water Research* **2018**, *139*, 329-352.
- 16. Su, C.; Horseman, T.; Cao, H.; Christie, K.; Li, Y.; Lin, S., Robust Superhydrophobic Membrane for Membrane Distillation with Excellent Scaling Resistance. *Environmental science & technology* **2019**, *53* (20), 11801-11809.
- 17. Karanikola, V.; Boo, C.; Rolf, J.; Elimelech, M., Engineered Slippery Surface to Mitigate Gypsum Scaling in Membrane Distillation for Treatment of Hypersaline Industrial Wastewaters. *Environmental science & technology* **2018**, *52* (24), 14362-14370.
- 18. Wang, Z.; Lin, S., Membrane fouling and wetting in membrane distillation and their mitigation by novel membranes with special wettability. *Water Research* **2017**, *112*, 38-47.
- 19. Boo, C.; Lee, J.; Elimelech, M., Omniphobic Polyvinylidene Fluoride (PVDF) Membrane for Desalination of Shale Gas Produced Water by Membrane Distillation. *Environmental Science & Technology* **2016**, *50* (22), 12275-12282.
- 20. Servi, A. T.; Guillen-Burrieza, E.; Warsinger, D. M.; Livernois, W.; Notarangelo, K.; Kharraz, J.; Lienhard, J. H.; Arafat, H. A.; Gleason, K. K., The effects of iCVD film thickness and conformality on the permeability and wetting of MD membranes. *Journal of Membrane Science* **2017**, *523*, 470-479.

- 21. Servi, A. T.; Kharraz, J.; Klee, D.; Notarangelo, K.; Eyob, B.; Guillen-Burrieza, E.; Liu, A.; Arafat, H. A.; Gleason, K. K., A systematic study of the impact of hydrophobicity on the wetting of MD membranes. *Journal of Membrane Science* **2016**, *520*, 850-859.
- 22. Warsinger, D. M.; Servi, A.; Van Belleghem, S.; Gonzalez, J.; Swaminathan, J.; Kharraz, J.; Chung, H. W.; Arafat, H. A.; Gleason, K. K., Combining air recharging and membrane superhydrophobicity for fouling prevention in membrane distillation. *Journal of membrane science* **2016**, *505*, 241-252.
- 23. Gryta, M., Influence of polypropylene membrane surface porosity on the performance of membrane distillation process. *Journal of Membrane Science* **2007**, *287* (1), 67-78.
- 24. Gupta, M.; Gleason, K. K., Initiated chemical vapor deposition of poly (1H, 1H, 2H, 2H-perfluorodecyl acrylate) thin films. *Langmuir* **2006**, *22* (24), 10047-10052.
- 25. Erbil, H. Y.; Demirel, A. L.; Avcı, Y.; Mert, O., Transformation of a simple plastic into a superhydrophobic surface. *Science* **2003**, *299* (5611), 1377-1380.
- Sadeghi, I.; Govinna, N.; Cebe, P.; Asatekin, A., Superoleophilic, Mechanically Strong Electrospun Membranes for Fast and Efficient Gravity-Driven Oil/Water Separation. *Acs Applied Polymer Materials* **2019**, *1* (4), 765-776.
- 27. Tian, Y.; Jiang, L., Wetting: Intrinsically robust hydrophobicity. *Nature materials* **2013**, *12* (4), 291.
- 28. Munirasu, S.; Banat, F.; Durrani, A. A.; Haija, M. A., Intrinsically superhydrophobic PVDF membrane by phase inversion for membrane distillation. *Desalination* **2017**, *417*, 77-86.
- 29. Wang, Z.; Tang, Y.; Li, B., Excellent wetting resistance and anti-fouling performance of PVDF membrane modified with superhydrophobic papillae-like surfaces. *Journal of Membrane Science* **2017**, *540*. 401-410.
- 30. Li, X.; Wang, C.; Yang, Y.; Wang, X.; Zhu, M.; Hsiao, B. S., Dual-biomimetic superhydrophobic electrospun polystyrene nanofibrous membranes for membrane distillation. *ACS applied materials & interfaces* **2014**, 6 (4), 2423-2430.
- 31. Liao, Y.; Loh, C.-H.; Wang, R.; Fane, A. G., Electrospun superhydrophobic membranes with unique structures for membrane distillation. *ACS applied materials & interfaces* **2014**, *6* (18), 16035-16048.
- 32. Guo, F.; Servi, A.; Liu, A.; Gleason, K. K.; Rutledge, G. C., Desalination by membrane distillation using electrospun polyamide fiber membranes with surface fluorination by chemical vapor deposition. *ACS applied materials & interfaces* **2015**, *7* (15), 8225-8232.
- 33. Dong, Z.-Q.; Wang, B.-J.; Ma, X.-h.; Wei, Y.-M.; Xu, Z.-L., FAS grafted electrospun poly (vinyl alcohol) nanofiber membranes with robust superhydrophobicity for membrane distillation. *ACS applied materials & interfaces* **2015**, *7* (40), 22652-22659.
- 34. Dong, Z.-Q.; Ma, X.-H.; Xu, Z.-L.; Gu, Z.-Y., Superhydrophobic modification of PVDF–SiO 2 electrospun nanofiber membranes for vacuum membrane distillation. *RSC Advances* **2015**, *5* (83), 67962-67970.
- 35. Hamzah, N.; Leo, C., Fouling prevention in the membrane distillation of phenolic-rich solution using superhydrophobic PVDF membrane incorporated with TiO2 nanoparticles. *Separation and Purification Technology* **2016**, *167*, 79-87.
- 36. Zhu, Z.; Liu, Y.; Hou, H.; Shi, W.; Qu, F.; Cui, F.; Wang, W., Dual-bioinspired design for constructing membranes with superhydrophobicity for direct contact membrane distillation. *Environmental science & technology* **2018**, *52* (5), 3027-3036.
- 37. Cong, S.; Guo, F., Janus Nanofibrous Membranes for Desalination by Air Gap Membrane Distillation. *Acs Applied Polymer Materials* **2019**, *1* (12), 3443-3451.
- 38. Meng, S.; Ye, Y.; Mansouri, J.; Chen, V., Fouling and crystallisation behaviour of superhydrophobic nano-composite PVDF membranes in direct contact membrane distillation. *Journal of Membrane Science* **2014**, *463*, 102-112.
- 39. Meng, S.; Ye, Y.; Mansouri, J.; Chen, V., Crystallization behavior of salts during membrane distillation with hydrophobic and superhydrophobic capillary membranes. *Journal of Membrane Science* **2015**, *473*, 165-176.
- 40. Lu, K.-J.; Zuo, J.; Chung, T.-S., Tri-bore PVDF hollow fibers with a super-hydrophobic coating for membrane distillation. *Journal of Membrane Science* **2016**, *514*, 165-175.
- 41. Xiao, Z.; Zheng, R.; Liu, Y.; He, H.; Yuan, X.; Ji, Y.; Li, D.; Yin, H.; Zhang, Y.; Li, X.-M.; He, T., Slippery for scaling resistance in membrane distillation: a novel porous micropillared superhydrophobic surface. *Water Research* **2019**, *155*, 152-161.
- 42. Xiao, Z.; Li, Z.; Guo, H.; Liu, Y.; Wang, Y.; Yin, H.; Li, X.; Song, J.; Nghiem, L. D.; He, T., Scaling mitigation in membrane distillation: From superhydrophobic to slippery. *Desalination* **2019**, *466*, 36-43.

- 43. Drioli, E.; Ali, A.; Macedonio, F., Membrane distillation: Recent developments and perspectives. *Desalination* **2015.** *356*. 56-84.
- 44. Zha, F. F.; Fane, A. G.; Fell, C. J. D.; Schofield, R. W., Critical displacement pressure of a supported liquid membrane. *Journal of Membrane Science* **1992**, *75* (1), 69-80.
- 45. Guillen-Burrieza, E.; Servi, A.; Lalia, B. S.; Arafat, H. A., Membrane structure and surface morphology impact on the wetting of MD membranes. *Journal of Membrane Science* **2015**, *483* (Supplement C), 94-103.
- 46. Kim, B.-S.; Harriott, P., Critical entry pressure for liquids in hydrophobic membranes. *Journal of Colloid and Interface Science* **1987**, *115* (1), 1-8.
- 47. Mullin, J. W., Crystallization. Elsevier: 2001.
- 48. Curcio, E.; Fontananova, E.; Di Profio, G.; Drioli, E., Influence of the structural properties of poly (vinylidene fluoride) membranes on the heterogeneous nucleation rate of protein crystals. *The Journal of Physical Chemistry B* **2006**, *110* (25), 12438-12445.
- 49. Horseman, T.; Su, C.; Christie, K. S.; Lin, S., Highly Effective Scaling Mitigation in Membrane Distillation Using a Superhydrophobic Membrane with Gas Purging. *Environmental Science & Technology Letters* **2019**, *6* (7), 423-429.
- 50. Childress, A. E.; Elimelech, M., Effect of solution chemistry on the surface charge of polymeric reverse osmosis and nanofiltration membranes. *Journal of membrane science* **1996**, *119* (2), 253-268.
- 51. Wang, Z.; Chen, Y.; Lin, S., Kinetic model for surfactant-induced pore wetting in membrane distillation. *Journal of Membrane Science* **2018**, *564*, 275-288.
- 52. Rezaei, M.; Warsinger, D. M.; Lienhard V, J. H.; Samhaber, W. M., Wetting prevention in membrane distillation through superhydrophobicity and recharging an air layer on the membrane surface. *Journal of Membrane Science* **2017**, *530*, 42-52.
- 53. Chew, N. G. P.; Zhao, S.; Malde, C.; Wang, R., Superoleophobic surface modification for robust membrane distillation performance. *Journal of Membrane Science* **2017**, *541*, 162-173.
- 54. Huang, Y.-X.; Wang, Z.; Jin, J.; Lin, S., Novel Janus membrane for membrane distillation with simultaneous fouling and wetting resistance. *Environmental science & technology* **2017**, *51* (22), 13304-13310.
- 55. Lu, X.; Peng, Y.; Ge, L.; Lin, R.; Zhu, Z.; Liu, S., Amphiphobic PVDF composite membranes for anti-fouling direct contact membrane distillation. *Journal of Membrane Science* **2016**, *505*, 61-69.
- Park, H. B.; Kamcev, J.; Robeson, L. M.; Elimelech, M.; Freeman, B. D., Maximizing the right stuff: The trade-off between membrane permeability and selectivity. *Science* **2017**, *356* (6343), eaab0530.
- 57. OECD, Preliminary Lists of PFOS, PFAS, PFOA and Related Compounds and Chemicals that May Degrade to PFCA. *OECD Papers* **2006**, *6/11*.
- 58. Asatekin, A.; Gleason, K. K., Polymeric nanopore membranes for hydrophobicity-based separations by conformal initiated chemical vapor deposition. *Nano letters* **2010**, *11* (2), 677-686.
- 59. Latthe, S. S.; Gurav, A. B.; Maruti, C. S.; Vhatkar, R. S., Recent progress in preparation of superhydrophobic surfaces: a review. *Journal of Surface Engineered Materials and Advanced Technology* **2012**, *2* (02), 76.
- 60. Cheng, C.; Gupta, M., Roll-to-Roll Surface Modification of Cellulose Paper via Initiated Chemical Vapor Deposition. *Industrial & Engineering Chemistry Research* **2018**, *57* (34), 11675-11680.
- 61. McGaughey, A.; Gustafson, R.; Childress, A., Effect of long-term operation on membrane surface characteristics and performance in membrane distillation. *Journal of Membrane Science* **2017**, *543*, 143-150.
- Riche, C. T.; Marin, B. C.; Malmstadt, N.; Gupta, M., Vapor deposition of cross-linked fluoropolymer barrier coatings onto pre-assembled microfluidic devices. *Lab on a Chip* **2011**, *11* (18), 3049-3052.
- 63. Morra, M.; Occhiello, E.; Garbassi, F., Surface characterization of plasma-treated PTFE. *Surface and Interface Analysis* **1990**, *16* (1-12), 412-417.
- 64. Koyuncu, I.; Brant, J.; Lüttge, A.; Wiesner, M. R., A comparison of vertical scanning interferometry (VSI) and atomic force microscopy (AFM) for characterizing membrane surface topography. *Journal of Membrane Science* **2006**, *278* (1), 410-417.
- 65. Good, R.; Chaudhury, M.; Van Oss, C., Fundamentals of adhesion. LH Lee (Ed.) 1991, 153.
- 66. Jańczuk, B.; Białopiotrowicz, T., The total surface free energy and the contact angle in the case of low energetic solids. *Journal of colloid and interface science* **1990**, *140* (2), 362-372.
- 67. De Gennes, P.-G.; Brochard-Wyart, F.; Quéré, D., Capillarity and wetting phenomena: drops, bubbles, pearls, waves. Springer Science & Business Media: 2004.

- 68. Mejia Mendez, D. L.; Castel, C.; Lemaitre, C.; Favre, E., Membrane distillation (MD) processes for water desalination applications. Can dense selfstanding membranes compete with microporous hydrophobic materials? *Chemical Engineering Science* **2018**, *188*, 84-96.
- 69. Shaulsky, E.; Karanikola, V.; Straub, A. P.; Deshmukh, A.; Zucker, I.; Elimelech, M., Asymmetric membranes for membrane distillation and thermo-osmotic energy conversion. *Desalination* **2019**, *452*, 141-148.
- 70. Nejati, S.; Boo, C.; Osuji, C. O.; Elimelech, M., Engineering flat sheet microporous PVDF films for membrane distillation. *Journal of Membrane Science* **2015**, *492*, 355-363.